Received: 22 April 2022 | Revised: 7 July 2022 | Accepted: 21 July 2022

DOI: 10.1002/wcms.1634

FOCUS ARTICLE

WIREs COMPUTATIONAL MOLECULAR SCIENCE WILEY

Density functionals based on the mathematical structure of the strong-interaction limit of DFT

Stefan Vuckovic[1,2] | **Augusto Gerolin**[3,4] | **Timothy J. Daas**[2] | **Hilke Bahmann**[5] | **Gero Friesecke**[6] | **Paola Gori-Giorgi**[2]

[1]Institute for Microelectronics and Microsystems (CNR-IMM), Lecce, Italy

[2]Department of Chemistry & Pharmaceutical Sciences and Amsterdam Institute of Molecular and Life Sciences (AIMMS), Faculty of Science, Vrije Universiteit, Amsterdam, The Netherlands

[3]Department of Chemistry and Biomolecular Sciences, University of Ottawa, Ottawa, Ontario, Canada

[4]Department of Mathematics and Statistics, University of Ottawa, Ottawa, Ontario, Canada

[5]Physical and Theoretical Chemistry, University of Wuppertal, Wuppertal, Germany

[6]Department of Mathematics, Technische Universität München, Munich, Germany

Correspondence
Paola Gori-Giorgi, Department of Chemistry & Pharmaceutical Sciences and Amsterdam Institute of Molecular and Life Sciences (AIMMS), Faculty of Science, Vrije Universiteit, De Boelelaan 1083, 1081HV Amsterdam, The Netherlands.
Email: p.gorigiorgi@vu.nl

Stefan Vuckovic Institute for Microelectronics and Microsystems (CNR-IMM), 73100 Lecce Italy; Department of Chemistry & Pharmaceutical Sciences and Amsterdam Institute of Molecular and Life Sciences (AIMMS), Faculty of Science, Vrije Universiteit, De Boelelaan 1083, 1081HV Amsterdam, The Netherlands.
Email: stefanvuckovic1@gmail.com

Funding information
Canada Research Chairs, Grant/Award Number: RGPIN-2022-05207; Deutsche Forschungsgemeinschaft, Grant/Award Numbers: 418140043, CRC 109; Horizon Europe Marie Sklodowska-Curie Actions, Grant/Award Number: 101033630; Nederlandse Organisatie voor Wetenschappelijk Onderzoek, Grant/Award Number: 724.017.001

Edited by: Peter R. Schreiner, Editor-in-Chief

Abstract

While in principle exact, Kohn–Sham density functional theory—the workhorse of computational chemistry—must rely on approximations for the exchange–correlation functional. Despite staggering successes, present-day approximations still struggle when the effects of electron–electron correlation play a prominent role. The limit in which the electronic Coulomb repulsion completely dominates the exchange–correlation functional offers a well-defined mathematical framework that provides insight for new approximations able to deal with strong correlation. In particular, the mathematical structure of this limit, which is now well-established thanks to its reformulation as an optimal transport problem, points to the use of very different ingredients (or features) with respect to the traditional ones used in present approximations. We focus on strategies to use these new ingredients to build approximations for computational chemistry and highlight future promising directions.

This article is categorized under:

Electronic Structure Theory > Density Functional Theory

KEYWORDS

exchange–correlation functionals, optimal transport theory, strong electronic correlation

1 | INTRODUCTION

Owing to its high accuracy-to-cost ratio, Kohn–Sham density functional theory (KS DFT) is presently the primary building block of the successes of quantum chemistry in disciplines that stretch from biochemistry to materials science.[1–6] DFT calculations consume a significant fraction of the world's supercomputing power[7] and tens of thousands of scientific papers report DFT calculations with the number ever growing.[2] KS DFT is in principle exact, but in practice, it requires approximations to one piece of the total energy, the so-called exchange–correlation (XC) functional, which encodes the quantum, fermionic, and Coulombic nature of electrons.

The construction of modern XC approximations draws from different approaches. Some of them are based on forms fulfilling some known exact constraints,[1,8] some have been fitted to large databases,[3,5] and the most recent XC approximations are machine learned.[9–11] Regardless of these differences in their design, nearly all current DFT approximations are constructed from the same ingredients (or features) that form the "Jacob's ladder."[12,13]

Despite the progress,[10] state-of-the-art XC approximations have been greatly successful mainly in describing only weak and moderate electronic correlations.[3,4] The inability of state-of-the-art DFT to capture strong correlations hampers its reliability and predictive power.[1,2,6,14] Over the last two decades, the strongly interacting limit of DFT (SIL)[15–19] has been explored and a rigorous theory has been established. This theory reveals mathematical objects that are very different from the ingredients that are used for building standard XC approximations (semilocal quantities and KS orbitals forming the Jacob's ladder). By offering building blocks for XC functionals tailored to describe strong correlations, the SIL has a potential to solve the long-standing problem of DFT simulations of strong electronic correlations.

Here we give a summary of the development of the SIL in different contexts: the development of the theory itself, its practical realization, and the development of approximations drawing from it. We discuss paths for using this limit in different ways to solve the problem of strong correlations within DFT and discuss how it has enabled the construction of a range of quantities that can guide the further development of DFT. We also give an overview of how the SIL has motivated the development of methods that go beyond DFT, such as wavefunction methods delivering highly accurate noncovalent interactions.[20]

2 | EXCHANGE–CORRELATION FUNCTIONAL IN DFT

Using the Levy–Lieb (LL) constrained-search formalism[21,22] the ground state energy and density of a many-electron system in an external potential $v:\mathbb{R}^d \to \mathbb{R}$ can be obtained as

$$E_{\mathrm{GS}}[v] = \min_{\rho}\left\{F[\rho] + \int v(\mathbf{r})\rho(\mathbf{r})\mathrm{d}\mathbf{r}\right\}, \tag{1}$$

where $\rho(\mathbf{r})$ is the one-electron density, and where $F[\rho]$ is the $\lambda = 1$ (physical) value of the generalized universal LL functional for arbitrary coupling constant λ,

$$F^{\lambda}[\rho] = \min_{\Psi \mapsto \rho}\langle\Psi|\widehat{T} + \lambda\widehat{V}_{ee}|\Psi\rangle, \tag{2}$$

with $\widehat{T}$ the kinetic energy operator and $\widehat{V}_{ee}$ the electron–electron (Coulomb) repulsion operator. The physical dimension d is 3 but, as we will see in the following, it is also interesting to consider models when $d = 1$ or $d = 2$.

In Equation (2), the minimization is performed over all antisymmetric wavefunctions that integrate to $\rho(\mathbf{r})$, whereas the minimization in Equation (1) is performed over all N-representable densities.[21] In the Kohn–Sham formalism, the functional $F[\rho] = F^{\lambda=1}[\rho]$ is partitioned as

$$F[\rho] = T_s[\rho] + U[\rho] + E_{xc}[\rho], \tag{3}$$

where $T_s[\rho] = F^{\lambda=0}[\rho]$ is the KS non-interacting kinetic energy, $U[\rho]$ is the Hartree (mean-field) energy, and $E_{xc}[\rho]$ is the exchange–correlation energy. The adiabatic connection (AC) formula for the XC functional reads[23,24]

$$E_{xc}[\rho] = \int_0^1 W_\lambda[\rho] \mathrm{d}\lambda, \tag{4}$$

where $W_\lambda[\rho]$ is the global AC integrand:

$$W_\lambda[\rho] = \langle \Psi_\lambda[\rho] | \widehat{V}_{ee} | \Psi_\lambda[\rho] \rangle - U[\rho], \tag{5}$$

and $\Psi_\lambda[\rho]$ is the minimizing wavefunction in Equation (2). We can also write $W_\lambda[\rho]$ as

$$W_\lambda[\rho] = \int w_\lambda(\mathbf{r}) \rho(\mathbf{r}) \mathrm{d}\mathbf{r}, \tag{6}$$

where $w_\lambda(\mathbf{r})$ is a λ-dependent XC energy density (per particle) that is not uniquely defined. In the present work, we adhere to the definition in terms of the electrostatic potential of the XC hole (conventional DFT gauge),[25–28]

$$w_\lambda(\mathbf{r}) = \frac{1}{2} \int_0^\infty \frac{h_{\mathrm{xc}}^\lambda(\mathbf{r}, u)}{u} 4\pi u^2 \mathrm{d}u, \tag{7}$$

where $h_{\mathrm{xc}}^\lambda(\mathbf{r}, u)$ is the spherical average (over directions of $\mathbf{u} = \mathbf{r}' - \mathbf{r}$) of the XC hole around a given position $\mathbf{r}$. The XC hole, in turn, is determined by the pair density associated with the wavefunction $\Psi_\lambda[\rho]$.

3 | STRONGLY INTERACTING LIMIT OF DFT

In this section, we briefly review the physical ideas behind the strongly interacting limit of DFT. For a mathematically more rigorous and comprehensive overview, we recommend referring to Friesecke et al.[19]

The strongly interacting limit of DFT corresponds to the situation in which the electron–electron repulsion dominates in $F^\lambda[\rho]$ of Equation (2), namely[15,16]

$$\lim_{\lambda \to \infty} \frac{1}{\lambda} F^\lambda[\rho] = V_{ee}^{\mathrm{SCE}}[\rho], \tag{8}$$

where $V_{ee}^{\mathrm{SCE}}[\rho]$ is the *strictly correlated electrons (SCE) functional* defined by the minimization of the electronic repulsion over wavefunctions Ψ with density $\rho(\mathbf{r})$:

$$V_{ee}^{\mathrm{SCE}}[\rho] = \min_{\Psi \mapsto \rho} \langle \Psi | \widehat{V}_{ee} | \Psi \rangle. \tag{9}$$

The limit in Equation (8) has been established rigorously,[29–31] with the convergence of the "energies," that is, the value of the functional $F^\lambda[\rho]$ divided by λ tends to $V_{ee}^{\mathrm{SCE}}[\rho]$, and qualitative convergence of the wave-functions squared. More precisely, for any Ψ_λ minimizing (2), the spatial part of the N-body density obtained by summing over the spin degrees of freedom, $P_\lambda^N = \sum_{\mathrm{spins}} |\Psi_\lambda|^2$, in the $\lambda \to \infty$ limit, converges (after extraction of a subsequence) to a limiting N-body probability distribution $P_\infty^N[\rho]$ and convergence occurs in the sense that

$$\lim_{\lambda \to +\infty} \int_{\mathbb{R}^{dN}} g \sum_{s_1, \ldots, s_N} |\Psi_\lambda|^2 = \int_{\mathbb{R}^{dN}} g dP_\infty^N, \tag{10}$$

for all bounded continuous observables $g : \mathbb{R}^{dN} \to \mathbb{R}$ (mathematically: weak convergence of probability distributions). The limit state is concentrated on lower-dimensional sets, as discussed later.

The probability distribution $P_\infty^N[\rho]$ minimizes the following alternative definition of the SCE functional

$$V_{ee}^{\mathrm{SCE}}[\rho] = \min_{P^N \mapsto \rho} \sum_{i<j} \frac{1}{r_{ij}} P^N(\mathbf{r}_1, ..., \mathbf{r}_N) \mathrm{d}\mathbf{r}_1 ... \mathrm{d}\mathbf{r}_N, \tag{11}$$

where $r_{ij} = |\mathbf{r}_i - \mathbf{r}_j|$. Here the minimum is over all symmetric N-body probability distributions with one-body density ρ. Interestingly, unlike its absolute value squared, the wavefunction Ψ_λ itself does not converge to any meaningful limit. Since $P_\infty^N[\rho]$ minimizes only the electronic repulsion, one can think of it as a natural analog of the Kohn–Sham non-interacting state $\Psi_0[\rho]$, which minimizes the kinetic energy functional only. However, while with $\Psi_0[\rho]$ we can evaluate the expectation value of $\widehat{V}_{ee}$, we cannot evaluate the kinetic energy expectation value with $P_\infty^N[\rho]$. This can be done only through the next leading term of $F^{\lambda\to\infty}[\rho]$, which we discuss later.

3.1 | Links to the XC functional

The functional $V_{ee}^{\mathrm{SCE}}[\rho]$ also corresponds to a well-defined limit of the XC functional. In fact, the $\lambda \to \infty$ limit of the AC integrand of Equation (5) is equal to

$$W_\infty[\rho] = V_{ee}^{\mathrm{SCE}}[\rho] - U[\rho]. \tag{12}$$

Moreover, there is a well-known relationship[32,33] between scaling the coupling strength λ and performing uniform coordinate scaling on the density, $\rho_\gamma(\mathbf{r}) = \gamma^3 \rho(\gamma \mathbf{r})$ (with $\gamma > 0$), which implies that the exact XC functional tends to $W_\infty[\rho]$ in the low-density ($\gamma \to 0$) limit. The SCE limit is thus complementary to exchange, which yields the high-density limit ($\gamma \to \infty$) of $E_{xc}[\rho]$,

$$\lim_{\gamma\to\infty} \frac{E_{xc}[\rho_\gamma]}{\gamma} = E_x[\rho], \quad \lim_{\gamma\to 0} \frac{E_{xc}[\rho_\gamma]}{\gamma} = W_\infty[\rho]. \tag{13}$$

3.2 | The SCE state

As a candidate for the wave-function squared $P_\infty^N[\rho]$, Seidl and co-workers[15,16] proposed to restrict the minimization in (11) over singular distributions having the form:

$$\begin{aligned} P_{\mathrm{SCE}}^N = \frac{1}{N!} \sum_{\mathcal{P}} \int d\mathbf{s} \frac{\rho(\mathbf{s})}{N} \delta\big(\mathbf{r}_1 - \mathbf{f}_{\mathcal{P}(1)}(\mathbf{s})\big) \times \\ \times \delta\big(\mathbf{r}_2 - \mathbf{f}_{\mathcal{P}(2)}(\mathbf{s})\big) \times \cdots \times \delta\big(\mathbf{r}_N - \mathbf{f}_{\mathcal{P}(N)}(\mathbf{s})\big), \end{aligned} \tag{14}$$

where $\mathbf{f}_1, ..., \mathbf{f}_N$ are the so-called *co-motion functions*, with $\mathbf{f}_1(\mathbf{r}) = \mathbf{r}$, $\mathcal{P}$ is a permutation of {1,...N}, and $\delta(\mathbf{r} - \mathbf{f}_i(\mathbf{r}))$ denotes the delta function of $\mathbf{r}$ (alias Dirac measure) centered at $\mathbf{f}_i(\mathbf{r}) = \mathbf{f}_i([\rho];\mathbf{r})$. The singular distributions (14) are concentrated on the d-dimensional set $\Omega_0 \subset \mathbb{R}^{dN}$,

$$\Omega_0 = \{\mathbf{r}_1 = \mathbf{r}, \mathbf{r}_2 = f_2(\mathbf{r}), ..., \mathbf{r}_N = f_N(\mathbf{r})\}, \tag{15}$$

and its permutations. Intuitively speaking, such an N-body density describes a state in which the position of one of the electrons, say $\mathbf{r} \in \mathbb{R}^d$, can be freely chosen according to the density ρ, but this then uniquely fixes the position of all the other electrons through the *co-motion maps* $\mathbf{f}_i(\mathbf{r})$, that is, $\mathbf{r}_2 = f_2(\mathbf{r}), ..., \mathbf{r}_N = f_N(\mathbf{r})$. Thus states of form (14) are called *strictly correlated states*, or SCE states for short. In other words, if a reference electron is at $\mathbf{r}$, the other electrons in the

SCE state can be found nowhere else, but at the $\mathbf{f}_i(\mathbf{r})$ positions. Besides yielding minimal electronic repulsion, the co-motion functions need to satisfy group properties,[15,16,34] accounting for the indistinguishability of electrons, and the push forward condition, $\rho(\mathbf{f}_i(\mathbf{r}))\mathrm{d}\mathbf{f}_i(\mathbf{r}) = \rho(\mathbf{r})\mathrm{d}\mathbf{r}$, which ensures that the density constraint is met.[16,34]

Constructing the co-motion functions is not simple, except in some special cases such as one-dimensional and spherically symmetric systems.[15,16] In those cases, the co-motion maps are obtained from *constrained integrals of the density*. This is illustrated in Figure 1, which shows a simple one-dimensional example of the optimal solution for (9), which has the form (14), with strictly correlated positions separated by "chunks" of density that integrate into integers. We should stress that this solution has been rigorously proven to be exact for one-dimensional systems,[34] which means that in this case the exact XC functional in the low-density limit is entirely determined by these constrained integrals rather than by any of the traditional Jacob's ladder ingredients.

The SCE potential is defined as the functional derivative of the SCE functional $V_{ee}^{\mathrm{SCE}}[\rho]$ with respect to the density, $v_{\mathrm{SCE}}(\mathbf{r}) = \delta V_{ee}^{\mathrm{SCE}}[\rho]/\delta\rho(\mathbf{r})$, with the convention that $v_{\mathrm{SCE}}(\mathbf{r})$ tends to zero as $|\mathbf{r}| \to \infty$ for finite systems. Given an SCE state of Equation (14), the SCE functional and potential can be simply written in terms of the co-motion functions[35–37]:

$$V_{ee}^{\mathrm{SCE}}[\rho] = \int \frac{\rho(\mathbf{r})}{2} \sum_{i=2}^{N} \frac{1}{|\mathbf{r} - \mathbf{f}_i(\mathbf{r})|} \mathrm{d}\mathbf{r} \tag{16}$$

$$\nabla v_{\mathrm{SCE}}(\mathbf{r}) = -\sum_{i=2}^{N} \frac{\mathbf{r} - \mathbf{f}_i(\mathbf{r})}{|\mathbf{r} - \mathbf{f}_i(\mathbf{r})|^3}. \tag{17}$$

Equation (17) has a simple physical interpretation: $v_{\mathrm{SCE}}(\mathbf{r})$ is the one-body potential that corresponds to the net force exerted on an electron at position $\mathbf{r}$ by the other $N-1$ electrons.

Is the SCE state of Equation (14) actually always the *true* minimizer of Equation (11)? It has been proven that this is true when $N = 2$ in any dimension $d \geq 1$[18,29] and when $d = 1$ for any number of electrons.[34] In general, the SCE state of Equation (14) is not guaranteed to yield the absolute minimum for the electronic repulsion for a given arbitrary density $\rho(\mathbf{r})$.[38,39] This has been in-depth analyzed for spherically symmetric densities and it has been found that in the cases where the SCE solution is not optimal, $V_{\mathrm{ee}}^{\mathrm{SCE}}[\rho]$ of Equation (16) is still very close to the true minimum of Equation (11).[39]

3.3 | Other $V_{\mathrm{ee}}^{\mathrm{SCE}}[\rho]$ formulations

In addition to the co-motion functions formulation (Equation (16)), there are other equivalent formulations for $V_{ee}^{\mathrm{SCE}}[\rho]$ arising from mass transportation theory. The link between the SCE functional and mass transportation (or optimal

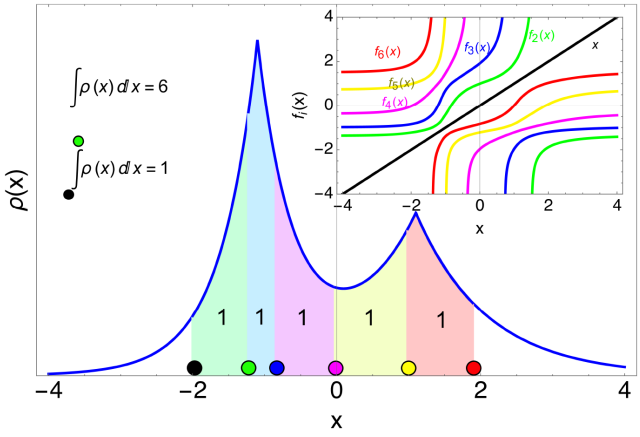

FIGURE 1 A pedagogical example: A sample of strictly correlated positions for a 1D density integrating to six electrons. A reference electron is placed at $x = -2$ (black point) and the SCE position of the other electron is determined by $f_i(x)$ and are represented by other colors. Notice that the shaded area between two adjacent SCE positions integrates to 1 and this is what defines $f_i(x)$ for 1D densities. Inset is showing the co-motion functions for the given density.

transport) theory was found, independently, by Buttazzo et al.[18] and by Cotar et al.[29] From the optimal transport viewpoint, the SCE functional defines a multimarginal problem, in which all the marginals are the same, so that the SCE mass-transportation problem corresponds to a reorganization of the "mass pieces" within the same density. From optimal transport theory, the dual Kantorovich formulation for $V_{ee}^{\mathrm{SCE}}[\rho]$ can be also deduced,[18]

$$V_{ee}^{\mathrm{SCE}}[\rho] = \max_{u} \left\{ \int u(\mathbf{r})\rho(\mathbf{r})\mathrm{d}\mathbf{r} : \sum_{i=1}^{N} u(\mathbf{r}_i) \leq \sum_{i<j} \frac{1}{|\,\mathbf{r}_i - \mathbf{r}_j\,|} \right\}, \tag{18}$$

defining the Kantorovich potential $u(\mathbf{r})$ as the maximizer of Equation (18). The same Equation (18) can be also reformulated[40] as a nested optimization:

$$V_{ee}^{\mathrm{SCE}}[\rho] = \max_{v_{\mathrm{SCE}}} \left\{ \int v_{\mathrm{SCE}}(\mathbf{r})\rho(\mathbf{r})\mathrm{d}\mathbf{r} + g[v_{\mathrm{SCE}}] \right\}, \tag{19}$$

where $g[v_{\mathrm{SCE}}]$ is the minimum of the classical potential energy,

$$E_{\mathrm{SCE}}^{\mathrm{pot}}(\mathbf{r}_1, ..., \mathbf{r}_N) = \sum_{i<j} \frac{1}{|\,\mathbf{r}_i - \mathbf{r}_j\,|} - \sum_{i=1}^{N} v_{\mathrm{SCE}}(\mathbf{r}_i), \tag{20}$$

over $\mathbf{r}_1, ..., \mathbf{r}_N$. In Equations (17) and (20), $v_{\mathrm{SCE}}(\mathbf{r})$ is defined up to a constant, which by convention is set such that $v_{\mathrm{SCE}}(\mathbf{r})$ tends to 0 as $|\,\mathbf{r}\,| \to \infty$ for finite systems. On the other hand, the constant in $u(\mathbf{r})$ is fixed by the linear constraints of Equation (18). For finite systems, this constant (equal to $u(\mathbf{r}) - v_{\mathrm{SCE}}(\mathbf{r})$) is exactly the strong-coupling limit of the Levy–Zahariev shift.[41,42]

3.4 | Next leading term

More information about the exact LL functional at low density can be gained by studying the next leading term in Equation (8). Under the assumption that the minimizer in (9) is of the SCE type (14), the classical potential energy (20) is minimum on the manifold Ω_0 parametrized by the co-motion functions. The conjecture is then that the next leading term is given by zero-point oscillations in the directions perpendicular to the SCE manifold[17]

$$F^{\lambda}[\rho] \underset{\lambda\to\infty}{\sim} \lambda V_{ee}^{\mathrm{SCE}}[\rho] + \sqrt{\lambda} F^{\mathrm{ZPE}}[\rho], \tag{21}$$

where ZPE stands for zero-point electronic energies, and where,

$$F^{\mathrm{ZPE}}[\rho] = \frac{1}{2}\int \frac{\rho(\mathbf{r})}{N} \mathrm{Tr}\left(\sqrt{\mathbb{H}(\mathbf{r})}\right) \mathrm{d}\mathbf{r}, \tag{22}$$

and $\mathbb{H}(\mathbf{r})$ is the hessian matrix composed of the second order derivatives of the SCE potential energy of Equation (20) evaluated at $\mathbf{r}_1 = \mathbf{r}, \mathbf{r}_2 = \mathbf{f}_2(\mathbf{r}), ...$ (i.e., on the manifold Ω_0 parametrized by the co-motion functions). The intuition that this next term should be given by zero-point oscillations around the manifold parametrized by the co-motion functions appeared for the first time in Seidl's seminal work,[15] and was later formalized, with calculations for small atoms (He to Ne) in Gori-Giorgi et al.[17] A rigorous proof in the one-dimensional case for any N has been provided recently.[43]

3.5 | The spin state

Besides the expansion of Equation (21) in terms of powers of λ, which is semiclassical in nature, it is conjectured[17,44] that the effect of the spin state will enter at large-λ through orders $e^{-\sqrt{\lambda}}$, which corresponds to the overlap of Gaussians centered in different co-motion functions. This conjecture has been confirmed numerically for $N = 2$ electrons in 1D.[45]

TABLE 1 An overview of proposed SCE algorithms

Algorithm	References	$N_{\max}$
SGS approach is based on co-motion functions (radial densities only)	50, see also 16 and 51	100
Linear programming applied to the N-body formulation (11)	39 and 52	3
Multi-marginal Sinkhorn algorithm	53–57	5
Algorithms based on the Kantorovich formulation (19)	40 and 42	6
Algorithm based on representability constraints for the pair density	58	10
Langevin dynamics with moment constraints	59 and 60	(To be assessed)
Genetic column generation (3D tests not yet available)	46	30

Note: The third column shows $N_{\max}$, which indicates up to how many electrons a given algorithm was applied to. This is not meant to be a direct comparison of methods as the reported results differ in the fineness of discretization and the accuracy achieved. Also, only the second, fourth and last algorithms are free of additional approximations beyond discretization.

3.6 | Numerical realization of the SCE functional

The SCE functional cannot at the moment be accurately and efficiently computed for general 3D densities and large N. But accurate numerical methods are available for small N or special situations, and novel methods aimed at large N are under development. In particular, the very recent genetic column generation method[46] appears in test examples to scale favorably with system size.

In Table 1, we give an overview of the proposed algorithms for computing the SCE functional and potential and refer to the book chapter[19] for a more detailed review. From Table 1, we can see that for general 3D densities, numerical solutions were reported only for up to 10 electrons (the first method is limited to radial densities, whereas for the last method 3D tests are not yet available). This indicates again the level of complexity and ultra nonlocality of the SCE functional.

In fact, in the worst-case scenario, the computational complexity of simple algorithms scales exponentially with the number N of electrons[47] and computing the SCE functional may be NP-hard.[46,48,49] In the discrete setting, where the single particle density ρ is supported on ℓ points, Equation (11) is equivalent to a linear programming problem with ℓN constraints and ℓ^N variables.

Despite these limitations in solving the SCE problem exactly, rather accurate approximations, retaining some of the SCE nonlocality, have been recently proposed and they will be detailed in the next section.

4 | APPROXIMATIONS TO THE SCE FUNCTIONAL

Existing approximations of the SCE functional are summarized in Table 2. They include the point-charge plus continuum (PC) model of Seidl and coworkers,[61] which has both a local density approximation (LDA) version and a gradient expansion version (GEA), and the recent harmonium PC (hPC) model, which is a generalized gradient approximation (GGA).[62] Notice that the PC model uses as LDA the idea of a spherical neutralizing cell around each electron, and its prefactor differs slightly from the exact SCE limit for a uniform density, given by the Madelung energy of the bcc Wigner crystal.[66] The nonlocal radius functional (NLR) and the shell model retain some of the SCE nonlocality[64,65] through the integrals of the spherically averaged density, which is defined as:

$$\widetilde{\rho}(\mathbf{r},u)=\frac{1}{4\pi}\int\rho(\mathbf{r}+\mathbf{u})\mathrm{d}\mathbf{\Omega}_{\mathbf{u}}. \tag{23}$$

NLR approximates the XC hole in the strong coupling limit whose depth (nonlocal radius), $u_1(\mathbf{r})$, is implicitly defined through the following integral, inspired by the exact SCE functional for 1D systems,

$$4\pi\int_0^{u_1(\mathbf{r})}u^2\widetilde{\rho}(\mathbf{r},u)\mathrm{d}u=1. \tag{24}$$

TABLE 2 Approximate $w_\infty(\mathbf{r})$ energy densities yielding $W_\infty[\rho]$ from: $W_\infty[\rho] = \int \rho(\mathbf{r}) w_\infty(\mathbf{r}) \mathrm{d}\mathbf{r}$

Approximation	$w_\infty(\mathbf{r})$ form	References
PC-LDA	$-\frac{9}{10}\left(\frac{4\pi}{3}\right)^{1/3}\rho(\mathbf{r})^{1/3}$	61
PC-GEA	$w_\infty^{\text{PC-LDA}}(\mathbf{r}) + 9\frac{2^{1/3}\pi}{175}\rho(\mathbf{r})^{1/3}s(\mathbf{r})^2$	61
GGA (hPC)	$w_\infty^{\text{PC-LDA}}(\mathbf{r})\frac{1+as(\mathbf{r})^2}{1+bs(\mathbf{r})^2}$	62
NLR	$-2\pi\int_0^{u_1(\mathbf{r})}\widetilde{\rho}(\mathbf{r},u)u\,\mathrm{d}u$	64
Shell model	$-2\pi\int_0^{u_s(\mathbf{r})}\widetilde{\rho}(\mathbf{r},u)u\,\mathrm{d}u + 2\pi\int_{u_s(\mathbf{r})}^{u_c(\mathbf{r})}\widetilde{\rho}(\mathbf{r},u)u\,\mathrm{d}u$	65

Note: PC stands for point-charge plus continuum (PC) model,[61] LDA stands for the local density approximation, GEA for the gradient expansion approximation, GGA for the generalized gradient approximation, and hPC[62] stands for the harmonium PC based on a GGA form,[63] whose parameters a and b are trained on the SCE energetics for the harmonium atom (for their numerical values see Ref. 62). The reduced density gradient, s, is given by $s(\mathbf{r}) = |\nabla\rho(\mathbf{r})|/\left(2(3\pi^2)^{1/3}\rho(\mathbf{r})^{4/3}\right)$. The nonlocal radius functional (NLR)[64] approximates the strong coupling limit of the XC hole, whose depth is given by Equation (24) and is calculated from the integrals over the spherically averaged density (Equation (23)). The shell model[65] adds a positive shell to the NLR hole, and the radii of the negative and positive shell, $u_s(\mathbf{r})$ and $u_c(\mathbf{r})$, respectively, are obtained at each $\mathbf{r}$ from the uniform electron gas constraint and the normalization constraint on the underlying XC hole. The approximate $w_\infty(\mathbf{r})$ from PC-LDA, NLR, and shell model are in the gauge of Equation (7) and thereby directly approximate $w_\infty(\mathbf{r})$ of Equation (26).

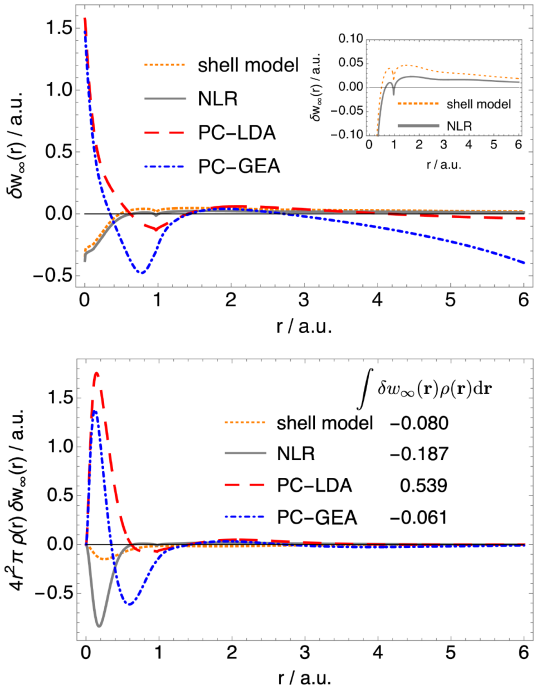

FIGURE 2 *Upper panel*: Difference between the exact (SCE) and approximate strong coupling limit energy density for the beryllium atom, $\delta w_\infty(\mathbf{r}) = w_\infty(\mathbf{r}) - w_\infty^{\text{model}}(\mathbf{r})$, as a function of the distance from the nucleus, r/a.u. The inset in the upper panel is focusing on the error of the shell and NLR model for larger r. *Lower panel*: The quantity from the upper panel multiplied by the density and the spherical volume element

Once $u_1(\mathbf{r})$ is computed, the energy density from the electrostatic potential of the NLR XC hole is computed, which in turn, defines $W_\infty[\rho]$ within NLR. The shell model is built upon NLR and makes it exact for the SCE limit of the uniform electron gas.[65]

In Figure 2, we explore the accuracy of different SCE approximations for energy densities (see Equation (26) below). From this figure, we can see that the shell model is the most accurate approximation locally. The PC-GEA model is the best performer globally here, and generally, it gives a rather accurate $W_\infty[\rho]$. However, the functional derivative of the PC-GEA diverges in the exponentially decaying density tails,[62,67,68] making self-consistent KS calculations impossible.

This problem is solved by turning to GGA's.[62,68] In particular, the very recently proposed hPC functional[62] preserves the accuracy of $W_\infty[\rho]$ from PC-GEA, while making self-consistent KS calculations possible.

In addition to the approximations for $W_\infty[\rho]$, the approximations for the next leading term, $F^{\mathrm{ZPE}}[\rho]$ (Equations (21) and (22)) have been also proposed. The most used[61,69–71] approximation to $F^{\mathrm{ZPE}}[\rho]$ is the one from the PC-GEA model,[61] which reads as:

$$F^{\mathrm{ZPE}}[\rho] \approx F^{\mathrm{ZPE}}_{\mathrm{PC}}[\rho] = 2\int \left[C\rho(\mathbf{r})^{3/2} + D\rho \frac{|\nabla\rho(\mathbf{r})|^2}{\rho(\mathbf{r})^{7/6}}, \right] \tag{25}$$

with $C = 1.535$ derived from the PC model,[61] and D typically set to 2.8957×10^{-2} by ensuring that $F^{\mathrm{ZPE}}_{\mathrm{PC}}[\rho]$ gives exact $F^{\mathrm{ZPE}}[\rho]$ for the helium atom.[17] In addition to PC-GEA, the very recent hPC model also provides a GGA form approximating $F^{\mathrm{ZPE}}[\rho]$.[62]

5 | FROM SCE TO PRACTICAL METHODS

The *bare* SCE functional is not directly applicable in chemistry as it over-correlates electrons. If we take the dissociation curve of H_2 as an example,[42,52] we can see that the SCE, unlike nearly all available XC approximations, dissociates the H_2 correctly without artificially breaking any symmetries, but predicts far too low energies around equilibrium and too short bond lengths. For this reason, SCE is not directly applicable in chemistry. Instead one should devise smarter strategies for incorporating the SCE in an approximate XC functional. The challenge is then to use the SCE information to equip new functionals with the ability to capture strong electronic correlations, while maintaining the accuracy of the standard DFT for weakly and moderately correlated systems. These strategies and challenges that come along the way are discussed in the following sections.

5.1 | Functionals via *global* interpolations between weak and strong coupling limit of DFT

XC approximations of different classes have been constructed from models to the global AC integrand (Equation (4)).[72–76] A possible way to avoid bias toward the weakly correlated regime present in nearly all XC approximations is to also include the information from the strongly interacting limit of $W_\lambda[\rho]$. Such an approach, called the interaction strength interpolation (ISI), where $W_\lambda[\rho]$ is obtained from an interpolation between its weakly and strongly interacting limits, has been proposed by Seidl and coworkers.[77] Since the ISI approach has been proposed, different interpolation forms with different input ingredients have been tested.[17,26,61,65,78–81] These approaches typically use the exact information from the weakly interacting limit [exact exchange and the correlation energy from the second-order Görling–Levy perturbation theory (GL2)[82]]. Except for some proof-of-principle calculations,[26,83,84] the ISI scheme uses the approximate ingredients from the large-λ limit ($W_\infty[\rho]$ and the next leading term described by $F^{\mathrm{ZPE}}[\rho]$) and these are typically modeled at a semilocal level. In some cases,[65,80] the ISI forms have been tested in tandem with the $W_\infty[\rho]$ approximations that retain some of the SCE nonlocality (see Section 4).

A potential problem of the ISI functionals is the lack of size consistency, which, however, can be easily corrected for interaction energies when there are no degeneracies.[85] The ISI functionals have been tested on several chemical data sets and systems and they perform reasonably well for interaction energies (energy differences).[69,71,85] When applied in the post-SCF fashion, the ISI approach seems more promising when used in tandem with Hartree–Fock (HF) than with semilocal Kohn–Sham orbitals. This finding has initiated the study of the strongly interacting limit in the Hartree–Fock theory[70,86] and the successes of approaches based on it will be briefly described in Section 5.5. Recently, the correlation potential from the ISI approach, which is needed for self-consistent ISI calculations to obtain the density and KS orbitals, has been computed.[67] It has been shown that it is rather accurate for a set of small atoms and diatomic molecules (see Figure 3, where we show that the ISI correlation potential provides a substantial improvement over that from GL2 for the neon atom).[67] The computed ISI correlation potentials have enabled fully self-consistent ISI calculations that have been recently reported in Śmiga et al.[62]

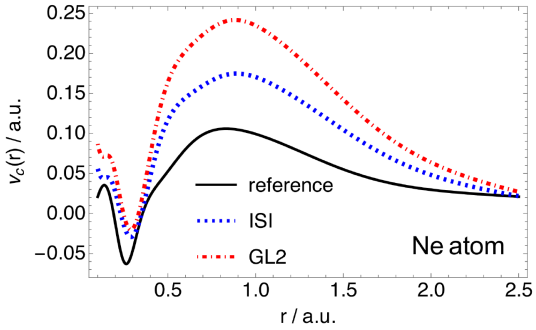

FIGURE 3 Correlation potentials v_c as a function of the distance from the nucleus (r) for the neon atom. The accurate correlation potential has been obtained from quantum Monte Carlo (QMC). All the data have been taken from Fabiano et al.[67]

5.2 | Functionals via *local* interpolations between weak and strong coupling limit of DFT

In addition to building models for the XC energy via global interpolations between the strongly and weakly interacting limits of $W_\lambda[\rho]$, one can also perform the interpolation locally (i.e., in each point of space).[26,81] This can be done by interpolating between the weakly and strongly interacting limits of $w_\lambda([\rho];\mathbf{r})$, which is the λ-dependent XC energy density of Equation (7). The main advantage of local interpolations[26,81,84] over their global counterparts is that the former are size-consistent by construction if the interpolation ingredients are size-consistent.[87,88] Thereby, local interpolations, unlike their global counterparts, do not require size-consistency correction.[28]

As mentioned earlier, there is no unique definition for $w_\lambda([\rho];\mathbf{r})$. Vuckovic et al.[28] explored the suitability of different definitions of the λ-dependent energy densities and it has been found that the energy densities definition of Equation (7) (electrostatic potential of the XC hole) is the best choice so far in this context. Within this definition, $w_\lambda([\rho];\mathbf{r})$ reduces to the exact exchange energy density when $\lambda = 0$, whereas in the $\lambda \to \infty$ (within the SCE formulation), it is defined in terms of the co-motion functions[35]:

$$w_\infty([\rho];\mathbf{r}) = \frac{1}{2}\sum_{i=2}^{N}\frac{1}{|\mathbf{r}-\mathbf{f}_i(\mathbf{r})|} - \frac{1}{2}v_H(\mathbf{r}), \tag{26}$$

where $v_H(\mathbf{r})$ is the Hartree potential. In addition to these two, a closed form expression for the local initial slope for $w_\lambda([\rho];\mathbf{r})$ has been derived in Vuckovic et al.[26] from second-order perturbation theory.

The accuracy of different local interpolation forms has been tested with both exact[26,84] and approximate[26,65,80] ingredients. Relative to the global interpolations, local interpolations typically give improved results for tested small chemical systems,[26] but usually do not fix the failures of global interpolations.[81] Nevertheless, the accuracy of XC functionals based on the local interpolation is still underexplored. This local interpolation framework can also be used to improve the latest XC approximations, such as the deep learned *local hybrids*,[10] especially when it comes to the treatment of strong electronic correlations.

5.3 | Fully nonlocal multiple radii functional—inspired by the exact SCE form

The mathematical form of the SCE functional has inspired new fully nonlocal approximations, called the multiple radii functional (MRF).[27,89,90] MRF approximates the XC energy densities of Equation (7) at arbitrary λ in the following way:

$$w_\lambda^{\mathrm{MRF}}(\mathbf{r}) = \frac{1}{2}\sum_{i=2}^{N}\frac{1}{R_i^\lambda([\rho];\mathbf{r})} - \frac{1}{2}v_H(\mathbf{r}). \tag{27}$$

Equation (27) can be thought of as the generalization of Equation (26), where starting from a reference electron at $\mathbf{r}$, the remaining electrons are assigned effective radii or distances from $\mathbf{r}$. The radii are then constructed from the integrals over the spherically averaged density and are implicitly defined by

$$4\pi \int_0^{R_i^\lambda(\mathbf{r})} u^2 \widetilde{\rho}(\mathbf{r}, u)\mathrm{d}u = i - 1 + \sigma_i^\lambda(\mathbf{r}), \tag{28}$$

where $\sigma_i^\lambda(\mathbf{r})$ is the so-called *fluctuation function*. The construction of the XC functional within MRF essentially reduces to building $\sigma_i^\lambda(\mathbf{r})$. So far, the main focus has been on building approximations for the $\lambda = 1$ case, and already very simple forms for $\sigma_i^{\lambda=1}(\mathbf{r})$ yield very accurate atomic $w_\lambda^{\mathrm{MRF}}(\mathbf{r})$ at the physical regime for atoms, while also accurately capturing the physics of stretched bonds. This shows that the forms inspired by the SCE can work for the physical regime if properly re-scaled. Furthermore, despite its full nonlocality, the cost of MRF is $O(N^3)$ within seminumerical schemes.[91]

By construction, MRF has very appealing properties: (1) it gives XC energies in the gauge of Equation (7) making it highly suitable to be used in the local interpolations described in Section 5.2; (2) these energy densities have the correct asymptotic behavior; (3) MRF captures the physics of bond breaking; (4) it is fully nonlocal so it can better describe the physics of strong electronic correlations that the usual semilocal DFT functionals; (5) its form is universal and does not change as dimensionality/interactions between particle changes as demonstrated in Gould and Vuckovic.[90] All these features of MRF and its flexibility make it very promising for building the next-generation of DFT approximations. There are ongoing efforts to transform these appealing features into robust XC functionals by developing improved MRF forms and efficiently implementing the MRF package into standard quantum-chemical codes.

5.4 | Other applications of SCE: Lower bounds to XC energies and correlation indicators

Besides being used to build XC approximations, the SCE approach has also proven very useful in understanding general features of the exact XC functional and the nature of electronic correlations. For example, the SCE limit is directly connected to the Lieb–Oxford (LO) inequality,[92,93] a key exact property used in the construction of XC approximations.[8,94] The LO inequality limits the value of the XC energy by bounding from below the AC integrand of Equation (5):

$$W_\lambda[\rho] \geq -C_{\mathrm{LO}} \int \rho^{4/3}(\mathbf{r})\mathrm{d}\mathbf{r}, \tag{29}$$

where the optimal C_{LO} is rigorously known to be between 1.4442 and 1.5765.[66,95,96] More generally, $-C_{\mathrm{LO}} \int \rho^{4/3}(\mathbf{r})\mathrm{d}\mathbf{r}$ bounds from below the indirect energy (electron–electron repulsion minus the Hartree energy) of *any* correctly normalized and antisymmetric $\Psi[\rho]$. Letting $\Psi[\rho]$ be $\Psi_\lambda[\rho]$, we obtain Equation (29). Since $W_\lambda[\rho]$ monotonically decreases with λ, $W_\infty[\rho]$ will be the smallest value for the l.h.s. of Equation (29). Thus, finding lower bounds for the optimal constant C_{LO} is equivalent to searching for densities ρ that maximize the ratio between $W_\infty[\rho]$ and $-\int \rho^{4/3}(\mathbf{r})\mathrm{d}\mathbf{r}$,[51,97] a procedure that has been applied to both the optimal C_{LO} for the general case and to the one for a specific number of electrons N.[28,51,97,98] An approach to tighten the lower bound to correlation energies for a given density has been also proposed by combining the adiabatic connection interpolation described in Section 5.1 and the SCE energies.[81]

In addition to provide tightened lower bounds for the XC energies, the SCE has also been used to define correlation indicators that quantify the ratio between *dynamical* and *static* correlation in a given system.[81] This idea has been also generalized to local indicators, enabling to visualize the interplay of dynamical and static correlation at different points in space.[81]

5.5 | Going beyond DFT—Large-λ limits in the Møller–Plesset adiabatic connection

The DFT AC introduced in Section 2, whose large λ limit is the focus of this article, defines the correlation energy in KS DFT. In a more traditional quantum-chemical sense, the correlation energy is defined as the difference between the true and Hartree–Fock (HF) energy. An exact expression for this correlation energy is given by the Møller–Plesset adiabatic connection (MPAC),[70] which connects the HF and physical state and has the Møller–Plesset

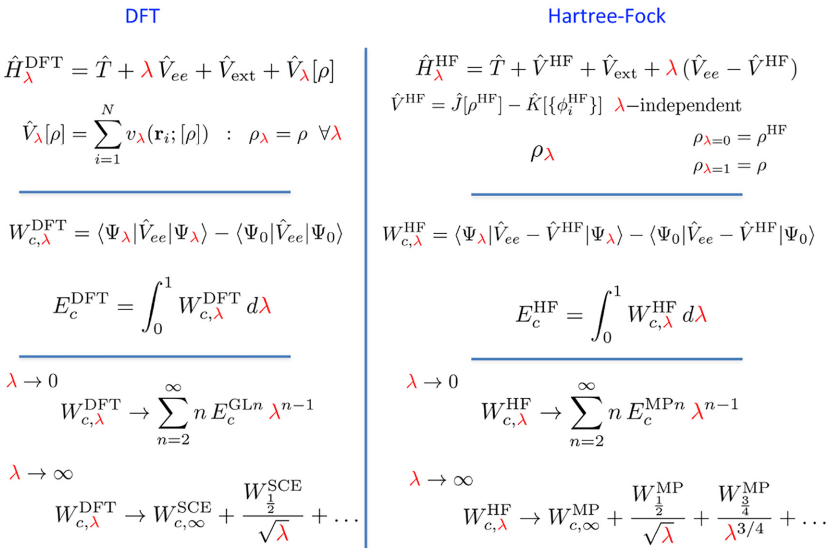

FIGURE 4 Two different adiabatic connections, linking the physical ($\lambda = 1$) system to either the KS or the Hartree–Fock determinant ($\lambda = 0$). *Left*: The density-fixed adiabatic connection of KS DFT (see Section 2). The Hamiltonian $\widehat{H}_\lambda^{\rm DFT}$ corresponds to Equation (2), with the one-body potential $v_\lambda(\mathbf{r})$ enforcing the constraint $\Psi_\lambda \mapsto \rho$, where ρ is the density of the physical system. The correlation part of the adiabatic connection integrand $W_{c,\lambda}^{\rm DFT}$ is equal to $W_\lambda[\rho]$ of Equation (5) minus $W_{\lambda=0}[\rho] = E_x[\rho]$. Small and large-$\lambda$ expansions for $W_{c,\lambda}^{\rm DFT}$ are also shown. *Right*: The adiabatic connection that has the Møller–Plesset (MP) series as a small perturbation expansion, considered in Section 5.5. The Hamiltonian $\widehat{H}_\lambda^{\rm HF}$ contains $\widehat{J}[\rho^{\rm HF}]$ and $\widehat{K}\left[\{\phi_i^{\rm HF}\}\right]$, which are the standard Hartree and exchange HF operators, respectively. The λ-dependent Ψ minimizing $\widehat{H}_\lambda^{\rm HF}$ has a density that changes with λ: At $\lambda = 0$ is equal to the HF density, while at $\lambda = 1$ is equal to the physical density. The expectation $W_{c,\lambda}^{\rm HF}$ is the AC integrand defining the correlation energy in HF theory. Small and large-λ expansions for $W_{c,\lambda}^{\rm HF}$ are also shown. The operator $\widehat{V}_{\rm ext}$ is the external (nuclear) potential

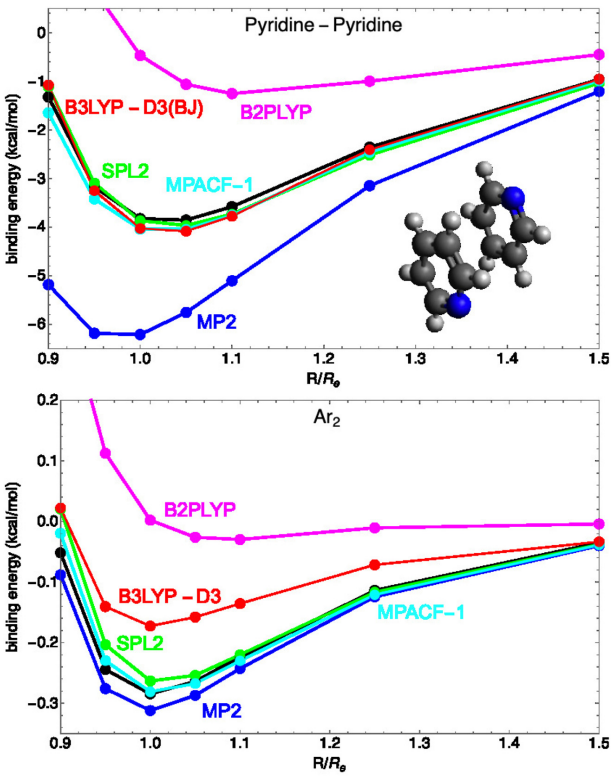

FIGURE 5 Dissociation curves of the pyridine (top) and argon dimers (bottom) obtained from MP2, SPL2, MPACF-1, B3LYP-D3, and B2PLYP with CCSD(T) (black line) as a reference

perturbation series as weak-interaction expansion. This AC is summarized and compared with the one of KS DFT used so far in this work in Figure 4. It has been recently shown that the large-λ limit of the MP AC is determined by functionals of the HF density.[70,86] Inequalities between the large-λ leading terms of the two AC's have been also established.[70,86]

The MP AC theory has been used to construct a predictor for the accuracy of MP2 for noncovalent interactions.[99] Methods that are based on the interpolation between the small and large λ limits of the MP AC have been also developed.[20] They are analogous to the ISI methods outlined in Section 5.1, which are used in the DFT context. It has been shown that these interpolation methods for the MP AC give very accurate results for noncovalent interactions.[20] We illustrate this in Figure 5, where we compare reference [CCSD(T)] to approximate dissociation curves from these interpolation approximations for the pyridine and argone dimers. The curves labeled SPL2 and MPACF-1 correspond to two new global interpolation forms[20] constructed by adding more flexibility and empirical parameters to the existing interpolation forms used in DFT[17,77] to capture the known exact features of the MP AC. For both of these noncovalently bound dimers, and for many other cases,[20] SPL2 and MPACF-1 show an excellent performance without using dispersion corrections. In general, they substantially improve over MP2 for noncovalent interactions, and are either on par with—or also improve—dispersion corrected (double) hybrids.[20]

6 | CONCLUSIONS AND OUTLOOK

Here we have reviewed the most important topics that the strongly interacting limit of DFT brings into focus. We have analyzed the development of different aspects of the underlying rigorous theory connecting DFT and optimal transport, and discussed how the SIL formulation influenced the development of different methods in DFT and beyond. Although this limit does not describe the physical regime, its mathematical structure contains essential elements pointing towards the real physics happening in molecular systems with strong correlations, whose description is one of the key unsolved problems in DFT. Thus, in the years and decades to come it will be very interesting to see how much the SIL ideas, formulations, and ensuing practical methods will be used to solve the strong correlation problem and to build the next generation of DFT methods. In particular, the new ingredients appearing in this limit can be used as new features to machine learn the XC functional.[9–11]

AUTHOR CONTRIBUTIONS

Stefan Vuckovic: Conceptualization (lead); formal analysis (equal); investigation (equal); methodology (equal); supervision (equal); validation (equal); visualization (equal); writing – original draft (lead); writing – review and editing (lead). **Augusto Gerolin:** Conceptualization (equal); formal analysis (equal); methodology (equal); project administration (equal); supervision (equal); validation (equal); visualization (equal); writing – original draft (equal); writing – review and editing (equal). **Timothy J. Daas:** Data curation (equal); validation (equal); visualization (equal); writing – original draft (equal); writing – review and editing (equal). **Hilke Bahmann:** Data curation (equal); methodology (equal); validation (equal); visualization (equal); writing – review and editing (equal). **Gero Friesecke:** Conceptualization (equal); formal analysis (equal); validation (equal); writing – original draft (equal); writing – review and editing (equal). **Paola Gori-Giorgi:** Conceptualization (equal); supervision (lead); writing – original draft (equal); writing – review and editing (equal).

ACKNOWLEDGMENTS

Stefan Vuckovic acknowledges funding from the Marie Sklodowska–Curie grant 101033630 (EU's Horizon 2020 programme). Augusto Gerolin acknowledges the support of his research by the Canada Research Chairs Program and Natural Sciences and Engineering Research Council of Canada (NSERC), funding reference number RGPIN-2022-05207. Hilke Bahmann acknowledges funding by the Deutsche Forschungsgemeinschaft (DFG, German Research Foundation) project no. 418140043. Timothy J. Daas and Paola Gori-Giorgi were supported by the Netherlands Organization for Scientific Research (NWO) under Vici grant 724.017.001. Gero Friesecke was partially supported by the Deutsche Forschungsgemeinschaft (DFG, German Research Foundation) through CRC 109.

CONFLICT OF INTEREST

All the authors declare to have no conflict of interest.

DATA AVAILABILITY STATEMENT

Data sharing is not applicable to this article as no new data were created or analyzed in this study.

ORCID

Stefan Vuckovic https://orcid.org/0000-0002-0768-9176
Augusto Gerolin https://orcid.org/0000-0002-2573-900X
Hilke Bahmann https://orcid.org/0000-0001-9144-8748
Paola Gori-Giorgi https://orcid.org/0000-0002-5952-1172

RELATED WIREs ARTICLE

Range-separated multiconfigurational density functional theory methods

REFERENCES

1. Burke K. Perspective on density functional theory. J Chem Phys. 2012;136(15):150901.
2. Pribram-Jones A, Gross DA, Burke K. DFT: a theory full of holes? Annu Rev Phys Chem. 2015;66(1):283–304. https://doi.org/10.1146/annurev-physchem-040214-121420
3. Mardirossian N, Head-Gordon M. Thirty years of density functional theory in computational chemistry: an overview and extensive assessment of 200 density functionals. Mol Phys. 2017;115(19):2315–72.
4. Goerigk L, Hansen A, Bauer C, Ehrlich S, Najibi A, Grimme S. A look at the density functional theory zoo with the advanced GMTKN55 database for general main group thermochemistry, kinetics and noncovalent interactions. Phys Chem Chem Phys. 2017;19(48):32184–215.
5. Verma P, Truhlar DG. Status and challenges of density functional theory. Trends Chem. 2020;2(4):302–18.
6. Sim E, Song S, Vuckovic S, Burke K. Improving results by improving densities: density-corrected density functional theory. J Am Chem Soc. 2022;144(15):6625–39. https://doi.org/10.1021/jacs.1c11506
7. Sherrill CD, Manolopoulos DE, Martínez TJ, Michaelides A. Electronic structure software. J Chem Phys. 2020;153(7):070401. https://doi.org/10.1063/5.0023185
8. Sun J, Ruzsinszky A, Perdew JP. Strongly constrained and appropriately normed semilocal density functional. Phys Rev Lett. 2015;115(3):036402.
9. Kalita B, Li L, McCarty RJ, Burke K. Learning to approximate density Functionals. Acc Chem Res. 2021;54(4):818–26. https://doi.org/10.1021/acs.accounts.0c00742
10. Kirkpatrick J, McMorrow B, Turban DH, Gaunt AL, Spencer JS, Matthews AG, et al. Pushing the frontiers of density functionals by solving the fractional electron problem. Science. 2021;374(6573):1385–9.
11. Nagai R, Akashi R, Sugino O. Completing density functional theory by machine learning hidden messages from molecules. NPJ Comput Mater. 2020;6(1):1–8. https://doi.org/10.1038/s41524-020-0310-0
12. Perdew JP, Schmidt K. Jacob's ladder of density functional approximations for the exchange-correlation energy. AIP Conference Proceedings. Volume 577. College Park, MD: AIP; 2001. p. 1–20.
13. Hammes-Schiffer S. A conundrum for density functional theory. Science. 2017;355(6320):28–9.
14. Cohen AJ, Mori-Sánchez P, Yang W. Challenges for density functional theory. Chem Rev. 2012;112:289–320.
15. Seidl M. Strong-interaction limit of density-functional theory. Phys Rev A. 1999;60:4387–95.
16. Seidl M, Gori-Giorgi P, Savin A. Strictly correlated electrons in density-functional theory: a general formulation with applications to spherical densities. Phys Rev A. 2007;75:042511.
17. Gori-Giorgi P, Vignale G, Seidl M. Electronic zero-point oscillations in the strong-interaction limit of density functional theory. J Chem Theory Comput. 2009;5:743–53.
18. Buttazzo G, De Pascale L, Gori-Giorgi P. Optimal-transport formulation of electronic density-functional theory. Phys Rev A. 2012;85(6):062502.
19. Friesecke G, Gerolin A, Gori-Giorgi P. The strong-interaction limit of density functional theory. In: Cances E, Friesecke G, editors. Density functional theory. New York: Springer Verlag; 2022.
20. Daas TJ, Fabiano E, Della Sala F, Gori-Giorgi P, Vuckovic S. Noncovalent interactions from models for the Møller–Plesset adiabatic connection. J Phys Chem Lett. 2021;12(20):4867–75.
21. Levy M. Universal variational functionals of electron densities, first-order density matrices, and natural spin-orbitals and solution of thev-representability problem. Proc Natl Acad Sci USA. 1979;76:6062–5.
22. Lieb EH. Density functionals for coulomb systems. Int J Quantum Chem. 1983;24:243–77.
23. Langreth DC, Perdew JP. The exchange-correlation energy of a metallic surface. Solid State Commun. 1975;17:1425–9.
24. Gunnarsson O, Lundqvist BI. Exchange and correlation in atoms, molecules, and solids by the spin-density-functional formalism. Phys Rev B. 1976;13:4274–98.
25. Burke K, Cruz FG, Lam KC. Unambiguous exchange-correlation energy density. J Chem Phys. 1998;109:8161–7.
26. Vuckovic S, Irons TJP, Savin A, Teale AM, Gori-Giorgi P. Exchange–correlation functionals via local interpolation along the adiabatic connection. J Chem Theory Comput. 2016;12(6):2598–610.

27. Vuckovic S, Gori-Giorgi P. Simple fully nonlocal density Functionals for electronic repulsion energy. J Phys Chem Lett. 2017;8(13): 2799–805.
28. Vuckovic S, Levy M, Gori-Giorgi P. Augmented potential, energy densities, and virial relations in the weak-and strong-interaction limits of DFT. J Chem Phys. 2017;147(21):214107.
29. Cotar C, Friesecke G, Klüppelberg C. Density functional theory and optimal transportation with coulomb cost. Comm Pure Appl Math. 2013;66:548–99.
30. Bindini U, De Pascale L. Optimal transport with coulomb cost and the semiclassical limit of density functional theory. J École Polytech Math. 2017;4:909–34. https://doi.org/10.5802/jep.59
31. Cotar C, Friesecke G, Klüppelberg C. Smoothing of transport plans with fixed marginals and rigorous semiclassical limit of the Hohenberg–Kohn functional. Arch Ration Mech Anal. 2018;228(3):891–922.
32. Levy M, Perdew JP. Hellmann-Feynman, virial, and scaling requisites for the exact universal density functionals. Shape of the correlation potential and diamagnetic susceptibility for atoms. Phys Rev A. 1985;32:2010–21.
33. Levy M, Perdew JP. Tight bound and convexity constraint on the exchange-correlation-energy functional in the low-density limit, and other formal tests of generalized-gradient approximations. Phys Rev B. 1993;48:11638–45.
34. Colombo M, De Pascale L, Di Marino S. Multimarginal optimal transport maps for one-dimensional repulsive costs. Can J Math. 2015; 5(67):350–68.
35. Mirtschink A, Seidl M, Gori-Giorgi P. Energy densities in the strong-interaction limit of density functional theory. J Chem Theory Comput. 2012;8(9):3097–107.
36. Malet F, Gori-Giorgi P. Strong correlation in Kohn-Sham density functional theory. Phys Rev Lett. 2012;109:246402.
37. Malet F, Mirtschink A, Cremon JC, Reimann SM, Gori-Giorgi P. Kohn-Sham density functional theory for quantum wires in arbitrary correlation regimes. Phys Rev B. 2013;87:115146.
38. Colombo M, Stra F. Counterexamples in multimarginal optimal transport with coulomb cost and spherically symmetric data. Math Models Methods Appl Sci. 2016;26(6):1025–49.
39. Seidl M, Di Marino S, Gerolin A, Nenna L, Giesbertz KJ, Gori-Giorgi P. The strictly-correlated electron functional for spherically symmetric systems revisited. arXiv. 2017;2017:170205022.
40. Mendl CB, Lin L. Kantorovich dual solution for strictly correlated electrons in atoms and molecules. Phys Rev B. 2013;87:125106.
41. Levy M, Zahariev F. Ground-state energy as a simple sum of orbital energies in Kohn-sham theory: a shift in perspective through a shift in potential. Phys Rev Lett. 2014;113:113002.
42. Vuckovic S, Wagner LO, Mirtschink A, Gori-Giorgi P. Hydrogen molecule dissociation curve with Functionals based on the strictly correlated regime. J Chem Theory Comput. 2015;11(7):3153–62.
43. Colombo M, Di Marino S, Stra F. First order expansion in the semiclassical limit of the Levy-Lieb functional. arXiv. 2021;2021: 210606282.
44. Gori-Giorgi P, Seidl M, Vignale G. Density-functional theory for strongly interacting electrons. Phys Rev Lett. 2009;103:166402.
45. Grossi J, Kooi DP, Giesbertz KJH, Seidl M, Cohen AJ, Mori-Sánchez P, et al. Fermionic statistics in the strongly correlated limit of density functional theory. J Chem Theory Comput. 2017;13:6089–100.
46. Friesecke G, Schulz AS, Vögler D. Genetic column generation: fast computation of high-dimensional multi-marginal optimal transport problems. SIAM J Sci Comp. 2021;44:A1632-A1654.
47. Lin T, Ho N, Cuturi M, Jordan MI. On the complexity of approximating multimarginal optimal transport. arXiv. 2019;2019:191000152.
48. Altschuler J, Boix-Adserà E. Polynomial-time algorithms for multimarginal optimal transport problems with structure. arXiv. 2020;2020: 200803006v1.
49. Altschuler JM, Boix-Adsera E. Hardness results for multimarginal optimal transport problems. Discr Optim. 2021;42:100669.
50. Vuckovic, S. Fully nonlocal exchange-correlation functionals from the strongcoupling limit of density functional theory. PhD thesis, 2017.
51. Seidl M, Vuckovic S, Gori-Giorgi P. Challenging the Lieb–Oxford bound in a systematic way. Mol Phys. 2016;114:1076–85.
52. Chen H, Friesecke G, Mendl CB. Numerical methods for a Kohn-Sham density functional model based on optimal transport. J Chem Theory Comput. 2014;10:4360–8.
53. Benamou JD, Carlier G, Cuturi M, Nenna L, Peyré G. Iterative bregman projections for regularized transportation problems. SIAM J Sci Comput. 2015;37(2):A1111–38.
54. Benamou JD, Carlier G, Nenna L. Splitting Methods in Communication, Imaging, Science, and Engineering. Cham: Springer; 2016.
55. Di Marino S, Gerolin A, Nenna L. Optimal transport for repulsive costs. In: Bergounioux M, Oudet É, Rumpf M, Carlier G, Champion T, Santambrogio F, editors. Topological optimization and optimal transport in the applied sciences. Berlin, Boston: De Gruyter; 2017.
56. Di Marino S, Gerolin A. An optimal transport approach for the Schrödinger bridge problem and convergence of Sinkhorn algorithm. J Sci Comput. 2020;85:27.
57. Gerolin A, Grossi J, Gori-Giorgi P. Kinetic correlation functionals from the entropic regularisation of the strictly-correlated electrons problem. J Chem Theory Comput. 2019;16(1):488–98.
58. Khoo Y, Ying L. Convex relaxation approaches for strictly correlated density functional theory. SIAM J Sci Comput. 2019;41(4):B773–95. https://doi.org/10.1137/18M1207478
59. Alfonsi A, Coyaud R, Ehrlacher V, Lombardi D. Approximation of optimal transport problems with marginal moments constraints. Math Comp. 2021;90:689–737.

60. Alfonsi A, Coyaud R, Ehrlacher V. Constrained overdamped Langevin dynamics for symmetric multimarginal optimal transportation. arXiv. 2021;2021:210203091.
61. Seidl M, Perdew JP, Kurth S. Density functionals for the strong-interaction limit. Phys Rev A. 2000;62:012502.
62. Śmiga S, Della Sala F, Gori-Giorgi P, Fabiano E. Self-consistent Kohn-Sham calculations with adiabatic connection models. arXiv. 2022; 2022:220211531.
63. Perdew JP, Burke K, Ernzerhof M. Generalized gradient approximation made simple. Phys Rev Lett. 1996;77:3865–8.
64. Wagner LO, Gori-Giorgi P. Electron avoidance: a nonlocal radius for strong correlation. Phys Rev A. 2014;90(5):052512.
65. Bahmann H, Zhou Y, Ernzerhof M. The shell model for the exchange-correlation hole in the strong-correlation limit. J Chem Phys. 2016;145(12):124104.
66. Lewin M, Lieb EH, Seiringer R. Floating Wigner crystal with no boundary charge fluctuations. Phys Rev B. 2019;100(3):035127.
67. Fabiano E, Śmiga S, Giarrusso S, Daas TJ, Della Sala F, Grabowski I, et al. Investigation of the exchange-correlation potentials of Functionals based on the adiabatic connection interpolation. J Chem Theory Comput. 2019;15:1006–15. https://doi.org/10.1021/acs.jctc.8b01037
68. Smiga S, Constantin LA. Modified interaction-strength interpolation method as an important step toward self-consistent calculations. J Chem Theory Comput. 2020;16(8):4983–92.
69. Fabiano E, Gori-Giorgi P, Seidl M, Della SF. Interaction-strength interpolation method for Main-group chemistry: benchmarking, limitations, and perspectives. J Chem Theory Comput. 2016;12(10):4885–96.
70. Seidl M, Giarrusso S, Vuckovic S, Fabiano E, Gori-Giorgi P. Communication: strong-interaction limit of an adiabatic connection in Hartree-Fock theory. J Chem Phys. 2018;149(24):241101. https://doi.org/10.1063/1.5078565
71. Giarrusso S, Gori-Giorgi P, Della Sala F, Fabiano E. Assessment of interaction-strength interpolation formulas for gold and silver clusters. J Chem Phys. 2018;148(13):134106.
72. Ernzerhof M. Construction of the adiabatic connection. Chem Phys Lett. 1996;263:499–506.
73. Burke K, Ernzerhof M, Perdew JP. The adiabatic connection method: a non-empirical hybrid. Chem Phys Lett. 1997;265:115–20.
74. Becke AD. Density-functional thermochemistry. III. The role of exact exchange. J Chem Phys. 1993;98:5648–52.
75. Mori-Sanchez P, Cohen AJ, Yang WT. Self-interaction-free exchange-correlation functional for thermochemistry and kinetics. J Chem Phys. 2006;124:091102.
76. Song S, Vuckovic S, Sim E, Burke K. Density sensitivity of empirical functionals. J Phys Chem Lett. 2021;12(2):800–7.
77. Seidl M, Perdew JP, Levy M. Strictly correlated electrons in density-functional theory. Phys Rev A. 1999;59:51–4.
78. Seidl M, Perdew JP, Kurth S. Simulation of all-order density-functional perturbation theory, using the second order and the strong-correlation limit. Phys Rev Lett. 2000;84:5070–3.
79. Liu ZF, Burke K. Adiabatic connection in the low-density limit. Phys Rev A. 2009;79:064503.
80. Zhou Y, Bahmann H, Ernzerhof M. Construction of exchange-correlation functionals through interpolation between the non-interacting and the strong-correlation limit. J Chem Phys. 2015;143:124103.
81. Vuckovic S, Irons TJP, Wagner LO, Teale AM, Gori-Giorgi P. Interpolated energy densities, correlation indicators and lower bounds from approximations to the strong coupling limit of DFT. Phys Chem Chem Phys. 2017;19:6169–83. https://doi.org/10.1039/C6CP08704C
82. Görling A, Levy M. Correlation-energy functional and its high-density limit obtained from a coupling-constant perturbation expansion. Phys Rev B. 1993;47:13105–13.
83. Malet F, Mirtschink A, Giesbertz KJH, Wagner LO, Gori-Giorgi P. Exchange-correlation functionals from the strong interaction limit of DFT: applications to model chemical systems. Phys Chem Chem Phys. 2014;16(28):14551–8.
84. Kooi DP, Gori-Giorgi P. Local and global interpolations along the adiabatic connection of DFT: a study at different correlation regimes. Theor Chem Acc. 2018;137(12):166.
85. Vuckovic S, Gori-Giorgi P, Della Sala F, Fabiano E. Restoring size consistency of approximate functionals constructed from the adiabatic connection. J Phys Chem Lett. 2018;9(11):3137–42.
86. Daas TJ, Grossi J, Vuckovic S, Musslimani ZH, Kooi DP, Seidl M, et al. Large coupling-strength expansion of the Møller–Plesset adiabatic connection: from paradigmatic cases to variational expressions for the leading terms. J Chem Phys. 2020;153(21):214112.
87. Gori-Giorgi P, Savin A. Degeneracy and size consistency in electronic density functional theory. J Phys: Conf Ser. 2008;117:012017.
88. Savin A. Is size-consistency possible with density functional approximations? Chem Phys. 2009;356:91–7.
89. Vuckovic S. Density functionals from the multiple-radii approach: analysis and recovery of the kinetic correlation energy. J Chem Theory Comput. 2019;15(6):3580–90.
90. Gould T, Vuckovic S. Range-separation and the multiple radii functional approximation inspired by the strongly interacting limit of density functional theory. J Chem Phys. 2019;151(18):184101.
91. Bahmann H, Kaupp M. Efficient self-consistent implementation of local hybrid Functionals. J Chem Theory Comput. 2015;11(4):1540–8.
92. Lieb EH. A lower bound for coulomb energies. Phys Lett. 1979;70A:444–6.
93. Lieb EH, Oxford S. Improved lower bound on the indirect coulomb energy. Int J Quantum Chem. 1981;19:427–39.
94. Perdew JP. In: Ziesche P, Eschrig H, editors. Electronic structure of solids. Berlin: Akademie Verlag; 1991.
95. Cotar C, Petrache M. Equality of the jellium and uniform electron gas next-order asymptotic terms for coulomb and Riesz potentials. arXiv. 2017;2017:170707664.
96. Lewin M, Lieb EH, Seiringer R. Improved Lieb-Oxford bound on the indirect and exchange energies. arXiv. 2022;2022:220312473.

97. Räsänen E, Seidl M, Gori-Giorgi P. Strictly correlated uniform electron droplets. Phys Rev B. 2011;83:195111.
98. Seidl M, Benyahia T, Kooi DP, Gori-Giorgi P. The Lieb-Oxford bound and the optimal transport limit of DFT. arXiv. 2022;2022: 220210800.
99. Vuckovic S, Fabiano E, Gori-Giorgi P, Burke K. MAP: an MP2 accuracy predictor for weak interactions from adiabatic connection theory. J Chem Theory Comput. 2020;16(7):4141–9.

How to cite this article: Vuckovic S, Gerolin A, Daas TJ, Bahmann H, Friesecke G, Gori-Giorgi P. Density functionals based on the mathematical structure of the strong-interaction limit of DFT. WIREs Comput Mol Sci. 2023;13(2):e1634. https://doi.org/10.1002/wcms.1634